Bone Regeneration by Hydroxyapatite-Gelatinnanocomposites

Sahar I Mostafa (sihmostafa@gmail.com)
Mansoura University Faculty of Science
Nesma M Abdelfattah
Mansoura University Faculty of Dentistry
Sayed M Ghorab
Mansoura University Faculty of Dentistry
Manal F Osman
Mansoura University Faculty of Dentistry
Noha A Elwassefy
Mansoura University Faculty of Dentistry

Research Article

Keywords: Hydroxyapatite, Gelatin, Alendronate, IBP nanocomposites, Cytotoxicity

Posted Date: August 16th, 2022

DOI: https://doi.org/10.21203/rs.3.rs-1934534/v1

Abstract

Aim of study:

Preparation and characterization of a series of new biocompatible injectable bone paste (IBP) nanocomposites, hydroxyapatite-gelatin (HA-Gel) and hydroxyapatite-Gelatin-alendronate (HA-Gel-Ald np).

Material and methods

IBP nanocomposites were synthesized from mixing different ratios of gelatin to aqueous solutions of both $Ca(NO_3)_2.4H_2O$ and $(NH_4)_2HPO_4$ to obtain (HA-Gel np), while the target nanocomposites, HA-Gel-Ald np, were obtained by submitting aqueous solution of alendronate (Ald) to HA-Gel np nanocomposites. These composites crystallinity were analyzed by FTIR and XRD, and their morphology were characterized by scanning electron microscopy (SEM) and EDX measurements. XRD patterns, SEM and EDX presented changes in the crystal and surface structure from HA to HA-Gel np to HA-Gel-Ald np. Furthermore, the cytotoxicity of the nanocomposites on stem cells were assessed using MTT assay.

Results

The physico-chemical measurements, FTIR, XRD, SEM and EDX indicated the success in isolating the nanocomposites, HA-Gel np and HA-Gel-Ald np, with different ratios. Although the cytotoxicity data show significant effect of the prepared IBP nanocomposites ($p = 0.00$), their interaction together had no significant effect ($p = 0.624$).

Introduction

Tissue engineering is considered as an interdisciplinary field, involves biomaterials science, cell biology, cell-material interactions and surface characterization, i.e., to enhance tissue functions [1]. Stem cell-based tissue engineering has the potential to revolutionize medicine with the ability to regenerate damaged and diseased tissues [2, 3].Scaffolds can be laden with cells for implantation [4]. Human bone marrow mesenchymal stem cells (HBMSCs) can be harvested from the patient, induced to differentiate into osteoblasts and combined with a scaffold to repair bone defects [5].

Osteoporosis is bone deformation disease in which bone mineral density (BMD) reduced, with micro-architecture disrupted, bone strength reduction and influenced by increasing of bone fracture risk [1, 6]. Osteoporosis is caused by an internal factor, reduction of bone ability to do bone remodeling process, due to unbalanced process of osteoblast and osteoclast, while bone defect is caused by external factor [7]. Osteoporosis could be treated by increasing the bone density or filling the bone defect with a suitable material.

Hydroxyapatite (HA; $Ca_{10}(PO_4)_6(OH)_2$; Fig. 1i) is a bioactive material, explored as a substitute for bone defect osteoporosis [8]. HA is fragile material and needs another support. Natural biopolymers (such as collagens, chitosan, gelatine, ..etc) have been widely used as biomaterials for bone tissue repair and engineering [9–12]. They increase osteoblast adhesion, migration, and mineralization.

Gel (Gel, derivative of collagen; Fig. 1ii) is a natural denatured polymer, composed of amino acids (hydroxyproline, proline, or sequences such as RGD – arginine-glycine-aspartic acid). It is known as a suitable biomaterial to mimic the extracellular matrix because of its function groups and the possibility to form 3D scaffolds with porous structure, i. e., it can be used in tissue engineering based on its biocompatibility and biodegradability [13, 14]. Gelatin-based scaffolds, such as polycaprolactone-58S bioactive glass-sodium/alginate-gelatin [15] and alginate-gelatin microspheres [13] have been prepared. Moreover, HA-Gel composite have been reported as a bone substitute material with high biocompatibility and non-toxicity [16].

Bone tissue is composed of a large number of calcium phosphate minerals (about 70%), collagen and polysaccharides (about 30%), thus, large number of research articles were focusing on applying composites of biodegradable natural polymers and bioactive ceramics, to mimic the extracellular matrix in the composition, avoid the brittleness of ceramics and low mechanical properties of polymers [17–20]. Gelatin particularly has always been used as the matrix of the composite due to its highly similar composition but lower costs than collagen, and hydroxyapatite (HA) nanoparticles have been selected as favorable fillers to reinforcethe composite [21–23]. Upon increasing HA nanoparticles content in HA-Gel composite would promote cell attachment, proliferation and increase levels of alkaline phosphatase and gene expression of osteogenic differentiation [24].

Bisphosphonates (Bps; Fig. 1iii) are important family of drugs for the treatment of bone tissue diseases, such as osteoporosis, bone metastases, hypercalcaemia and Paget's disease, due to their high affinity to the bone mineral hydroxyapatite [1, 25]. Bps are characterized by the [P-(R1) C (R2)-P unit] (Fig. 1), which allows a great number of possible variations, by changing the two lateral chains (R1 and R2) on the carbon atoms. The changes in R1 or R2 moiety can lead to extensive alterations in their physicochemical, biological, therapeutic and toxicological properties [26]. Extensive structure - activity studies showed useful drugs that combine potent inhibition of bone resorption osteoclastic action [27, 28]. Bps are significant and dose-dependent for osteo-blastogenesis [29]. Oral administration and intravenous injection have some adverse problems, such as gastrointestinal disorders, flu-like symptoms and low oral bioavailability. Therefore, it is necessary to improve the delivery method of Bps [30].

Bps drugs could be to help bone defect healing, like alendronate (Ald), which has high-affinity towards Ca^{2+} ions of HA, improve the interaction with bone calcium and inhibit the osteoclast in the bone engineering process [31].

Here in, we prepared a series of nanocomposite, HA-Gel np and HA-Gel-Ald np, by using different ratios of HA:Gel and (HA-Gel):Ald, respectively. The physical and chemical properties of the nanocomposites, and

their *In vitro* cytotoxicity were assessed. The composites showed positive effect on mesenchymal stem cell adhesion.

Materials And Methods

2.1. Material

All manipulations were performed under aerobic conditions using materials and solvents as received. Chemicals and solvents were obtained from sigma and merk. Calcium nitrate, Diammonium hydrogen phosphate, gelatin and Alendronate sodium trihydrate were purchased from Alfa Aesar (USA).

2.2. Instrumentation

Ultrasonication was performed on Digital ultrasonic bath CD-4830, 35 kHZ, China. The centrifuge apparatus used is Safety centrifuge Thermo Fisher Scientific Company, United States. FT-IR spectra were measured on a Matson5000 FT-IR spectrometer. SEM measurements were carried out using a Hitachi S-3000VP-SEM Variable Pressure-SEM. EDX measurement were performed using energy dispersive x-ray unit (EDX, JEOLJSM-5500LV SEM, JEOL Ltd, Japan) [32]. X-Ray powder diffraction patterns were assessed using X-ray diffractometer (XRD, PA-NalyticalX' Pert PRO, Netherlands, The Electron Microscope Unit, Mansoura University- Egypt) equipped with mono-chromatized Cu-Kα radiation (λ=1.542 Å, 50 kV and 40 mA). Sample analysis was covered the 2θ range from 4° to 80° at a scan rate of 0.02° sec^{-1} [33]. The size of the crystallites was calculated using the XRD data to determine the Full-Width Half Maximum (FWHM). Then, by applying Scherrer formula; {D, K, λ, B and θ are the crystallite size (nm),Scherer constant (0.9), the wavelength of X-rays (1.54056 A°), the line broadening at FWHM in radians, and the Bragg's angle in degrees, respectively) [34].

2.3. Preparation of IBP nanocomposites (HA-Gel np)

The IBP nanocomposites were prepared by chemical wet precipitation method.

2.3.1. Hydroxyapatite-Gelatin nanoparticles (HA-Gel np)

Aqueous solution of gelatin (0.616 g, 3.4 mmol; 100 mL) was added to hydrated $Ca(NO_3)_2.4H_2O$ (2.36 g, 10 mmol) in dist. water (20 mL). The reaction mixture was stirred to complete homogeneity and dissolution at 30° C. Subsequently, $(NH_4)_2HPO_4$ (0.78 g, 8 mmol) in water (100 mL) was added dropwise with vigorous stirring over the period of 30-45 min [35]. The reaction mixture was stirred for 24 hrs, and then kept without stirring overnight. The pH of the mixture was adjusted to ~9-10 by using ammonia solution and stand for another 48 hrs at room temperature. The precipitate was isolated by centrifugation for 5-10 min., washed repeatedly with dist. water, and finally dried at 50° C for 24 hrs [36].

Three groups of HA-Gel np composites were prepared in ratios; Group 1 (***G1***): HA-Gel 7:3 wt%; Group 2 (***G2***): HA-Gel 1:1 wt% and Group 3 (***G3***): HA-Gel 3:7 wt%.

2.3.2. Hydroxyapatite-gelatin-alendronate nanoparticles (HA-Gel-Ald np)

Hydrated sodium alendronate (0.25 g, 0.78 mmol; 10 mL) was added dropwise to HA-Gel np powders (0.5 g) under continuous stirring. The obtained mixture was kept stirring for 24 hrs at room temperature [37,38]. The obtained nanocomposites were filtered off, washed by ice-cold dist. water, and dried at 40^{o} C to constant weight.

The groups of HA-Gel-Ald np composites were produced in ratios; Group 4 (***G4***): (HA-Gel)-Ald7:3wt%; Group 5 (***G5***): (HA-Gel)-Ald1:1wt% and Group 6 (***G6***): (HA-Gel)-Ald 3:7wt%.

Note:

a) All the synthesized nanocomposites were selected in such amount that Ca/P molar ratio was maintained at 1.67 [39]

b) The IBP nanocomposites were manually pulverized using a mortar and pestle for fine powder formation [40].

2.4. Biological characterization and Cytotoxicity assay

In vitro cytotoxicity assays considered as indicators to measure the ability of cytotoxic compounds to cause cell damage or cell death. They are widely used in fundamental research and drug discovery for screening toxic compounds. MTT assay has been widely used to assess cell viability, based on the enzymatic reduction of 3-[4,5-dimethylthiazole-2-yl]-2,5-diphenyltetrazolium bromide (MTT) to MTT-formazan, which is catalyzed by mitochondrial succinate dehydrogenase [27]. Hence, the MTT assay is dependent on mitochondrial respiration and indirectly serves to assess the cellular energy capacity of a cell. It is a colorimetric reaction that can be measured from cell monolayers that have been plated in 35 mm dishes or multi well plates.

Disks of 5 mm diameter and 2 mm thickness were prepared by compressing the IBP nanocomposites powders into cylindrical mold. The disks were sterilized under UV-lamp for 3 hrs, washed 3 times with phosphate buffer saline, PSB (10 min for each wash).

The test was performed by using rat bone marrow mesenchymal stem cells (MSCs). The material was compressed in the form of discs and each disc was placed in in 96-well plates, followed by seeding of cells as suspension over the discs (5×10^3 cells in each well; the control was cells without any samples' disks). The micro well plate was incubated for 24 h at 37^{o} C. MTT solution was added onto each well and

incubated for 4 hours at 37° C. After incubation, 200 µl Dimethyl sulfoxide solution was added to each well and incubated for 15 minutes to dissolve the insoluble formazan. The measurement process was performed by Elisa reader showing the violet level as Optical Density (OD), which represents the cell viability of the material based on eq. 1 [41].

$$\textit{Cell viability}\ \% = \frac{\textit{Mean optical density} - \textit{blank optical density}}{\textit{Control optical density} - \textit{blank optical density}} \times 100. \qquad (1)$$

where, OD is the absorbance of sample when MSCs cells were seeded in a 96 well plate and treated with the leach liquor, while blank is the absorbance of the sample which only contained growth medium, and control was the absorbance of the sample which contained cells and growth medium.

Statistical analysis: Three repeated tests were performed in all the experiment and the results were presented as means ± standard deviation (SD). One-way analysis of variance (ANOVA) and Tukey's post hoc tests were used to compare between groups, while values with and without magnetic field were compared using Paired (dependent) test. A value of $p < 0.05$ was considered of statistical significance.

Results And Discussion

Gelatin (Gel; derivative of collagen) is a natural denatured polymer, composed of amino acids (hydroxyproline, proline, or sequences such as RGD – arginine-glycine-aspartic acid). Gel is known as a suitable biomaterial to mimic the extracellular matrix because its function groups and the possibility to form 3D scaffolds with porous structure, i. e., it can be used in tissue engineering based on its biocompatibility and biodegradability [15,41]. Gelatin-based scaffolds, such as polycaprolactone-58S bioactive glass-sodium/alginate-gelatin [42] and alginate-gelatin microspheres [15] have been prepared.

HA np (Ca/P molar ration 1.65 ± 0.1 and surface Ca/P atomic ratio 1.30 ± 0.05) has high affinity of interaction of positively charged Ca^{2+} with alendronate phosphate (PO_3^{2-})-richer surface groups [43].

3.1. FTIR spectral studies

FTIR spectral data are used to evaluate the functional groups of the synthesized composites {HA-Gel np (Fig. 2i) and HA-Gel-Ald np (Fig. 2ii)}. HA-Gel np nanocomposites are likely formed by the interaction between the critically small sized HA np and Gel molecule.[36]

The FTIR spectrum of HA np showed peaks at 1059 and 988 cm^{-1}, attributed to n_{as}(P-C-P) and n_s(P-C-P) stretching vibrations of phosphate groups, respectively [37], while that at 3568 cm^{-1} is due to n(OH) stretching vibration. Furthermore, bands at 678, 575, and 525 cm^{-1} were assigned to the d(O-P-O) bending of phosphate [24,37,44].

The spectrum of Gel shows two characteristic bands at 2923 and 2851 cm^{-1}, assigned to $n_{as}(CH_2)$ and $n_s(CH_2)$ stretching vibrations, and those at 1647 and 1558 cm^{-1} corresponding to $n_{as}(COO^-)$ and $n_s(COO^-)$ stretching vibrations of carboxylate group [24]. The band at 3433 cm^{-1} attributed to n(OH) stretching vibrations of hydrogen bond water. Two extra bands at 1683, 1537 and 1240 cm^{-1}belong to amide I (C=O), amide II (N-H) and amide III band {the plane of n(C-N) and d(N-H) group in amide) vibrations, respectively [45].

In the nanocomposite, HA-Gel np, and upon increasing Gel content (from G1 to G2 to G3), the intensities of IR bands of HA and Gel were increased, as well as the stretching vibration ofn(OH)based on H-bonds formation [24,45]. All G1 to G2 to G3 spectra exhibited broad band ~ 3100–3500 cm^{-1} due to n(OH) and n(NH) stretches [24]. In addition, the characteristic band of the amide I in free Gel was shifted to lower wavenumber (1655 cm^{-1}) in HA Gel np, indicating the electrostatic attraction interaction between Ca^{2+} ions (in HA) and O-C=O$^-$groups (in Gel) [46], causing elongation on C=O bond, with shift to lower wavenumber. All these features indicate the interaction between HA np and Gel to form HA-Gel np nanocomposites with different ratios [45,46].

In the FTIR spectrum of NaHAld, both n_{as}(P-C-P) and n_s(P-C-P) stretching vibrations were observed in the range of 800-655 cm^{-1} with the multiple bands in 3600–3300 cm^{-1} range, assigned to n(OH) stretching of P–OH and C–OH groups. The n_{as}(P-O) and n_s(P-O) stretching vibrations are observed at 1057 and (1021, 920) cm^{-1}, respectively, while the stretching and bending vibrations of P=O and P-OH groups giving rise to the bands in the fingerprint region below 1320 cm^{-1}. The bands at 1234 and 1183 cm^{-1} due to n(P=O) and n(P-O) stretches, respectively [47,48]. The spectrum shows also bands at 3350 and 3246 cm^{-1} attributed to $n_{as}(NH_2)$ and $n_s(NH_2)$, respectively [47].

The FTIR spectra of the composites HA-Gel-Ald np, broadening was observed in the bands at the1620, 1200–900 and 700–500 regions cm^{-1}, indicates the formation of interlinked bonds into the layer between hydroxyapatite PO_4^{-3} and P-OH/P-O bonds specific to Ald [49], and interaction between Ca^{2+} ions in HA and HPO_3^- anion of Ald^- [7].

3.2. X-Ray diffraction spectroscopy (XRD)

The nanocomposites, (HA-Gel np) were fabricated by using different ratios of HA:Gel (***G1***: 7:3; ***G2***: 1:1; ***G3***: 3:7 wt%, respectively. The XRD patterns of HA-Gel np were observed in Fig. 3. The XRD patterns of the fabricated HA np shows diffraction peaks with d-spacing values of 2q 26.30 and 32.03, 39.72,50.4, 51.4, and 59.9^o which are assigned to 210, 211, 130, 213, 321, 410, and 420 planes, respectively,i.e., d-spacing values matching with the hexagonal system with primitive lattice [50]. The crystalline phase of HA, based on the XRD diffraction peaks positions, is corresponding exactly to PDF card no. 09-0432 of HA. Gel is amorphous in nature, its XRD pattern exhibits single broad peak at 2q 21.04^o [24]. The XRD patterns of

HA-Gel np, show peaks at 2q21.00, 26.30 and 32.03, 39.72, 50.4, 51.4, and 59.9^{o}), indicating the presence of both HA np (at the same positions in free HA, with its original crystal structure) and Gel. Moreover, The XRD patterns indicate the formation of composite with crystallinity greatly affected the Gel content [51]. In case of HA-Gel-Ald np nanocomposite, the presence of Ald does not change the lattice constants of HA np phase [52]. The amorphous Gel patterns were interfered with the peaks of crystalline HA and Ald [17]. In addition, the increase of HA-Gel-Ald nps size in comparison to those of HA-Gel nps, may be attributed to the high affinity of Ald^{-} (HPO_3^{-}) to Ca^{2+} ions in HA, which form some pores with increasing its size [7]. The broadness of the XRD peaks indicate the lower in crystallinity upon adding Ald.

Table 1 lists the crystal sizes (nm) of HA-Gel np and HA-Gel-Ald np composites based on Scherer's equation (eq. 2) [53].

$$L = K\lambda / (\beta . \cos\theta) \qquad (2)$$

where, L and K are the nano crystallite size and is a dimensionless **shape factor, while** λ is the XRD radiation of wavelength (nm), β is the line broadening at half the maximum intensity and θ is the Bragg angle.

The addition of Ald greatly affected the composites crystal size, because of the interaction of Ca^{2+} ions in HA Ald^{-} anion, which may not alter the crystal structure of HA (Fig. 4). However, Ald^{-} anion affects the crystal dimensions and leads to definitely larger composite crystals' size [54,55].

3.3. Scanning electronic microscopy (SEM) &Energy dispersive X-ray (EDX) spectroscopy

The morphology of HA-Gel np nanocomposite was assessed *via* SEM analysis (Fig. 5). The porous structure of HA-Gel np is regular arrays of circular hollow channels with particle size of about 67.75 nm. When the HA-Gel was up to 7:3 ***(G1)***, the morphology of the surface showed apparent pores in comparison to the pure HA [26]. The porous structure may provide more space for cell growth. Upon adding more Gel, the HA np became more compact, since Gel filled the gaps between the HA np [26]. In the ratio HA-Gel (1:1; ***G2***), no pores were observed on the surface, while in case HA-Gel (3:7 ***G3***), HA np were barely observed on the surface. Upon adding Ald, the size was reduced with diameter of about 36 nm. In addition, Ald particles are randomly distributed in HA-Gel np matrix i.e. some are embedded in the pore wall and some are piled together between or within pores, reducing the pores size and shape [6].

It can be observed that a large amount of flaky deposition appeared on the surface, and to clarify the composition of these depositions, EDX analysis was subjected to demonstrate that the deposition mainly contains C, O, P and Ca elements. The elemental composition of HA, HA-Gel and HA-Gel-Ald was performed by EDX analysis (Fig. 6). HA np has 4.54 (C), 46.50 (O), 18.34 (P), 30.63 (Ca) wt% with Ca/P 1.67, while in case of HA-Gel np, 18.47 (C), 50.08 (O), 11.78 (P), 19.68 (Ca) wt% with Ca/P 1.67. In

case of HA-Gel-Ald np, Ca wt% decreased with increasing P wt%, with appearance of Na. The data show 17.16 (C), 45.27 (O), 0.88 (Na), 11.99 (P), 14.06 (Ca) wt% with Ca/P 1.17.

3.4. Biological characterization & Cytotoxicity assay

Rat bone marrow mesenchymal stem cells (MSCs) cells were used to evaluate the cytotoxicity assay of the fabricated compounds, HA np, HA-Gel nps (**G1, G2 and G3**) and HA-Gel-Ald nps (**G4, G5 and G6**), using MTT assay. Fig. 7 illustrates the obtained results. The absorbance at 570 nm represented the vitality of the MSCs cells in the MTT assay.

As reported in Tables 2 and 3, two ANOVA test revealed that the composition variable had a significant effect on the crystal size ($p = 0.00$). The concentration, composition and interaction of composition and concentration variable have significant effects ($p = 0.00$).

After MSCs cells were cultured in leach liquor of HA-Gel nps and HA-Gel-Ald np, the cells viability of were around 74 and 94%, respectively. These data showed that the fabricated nanocomposites with low toxicity and could be used as preliminary estimate for the proliferation tests of MSCs on the materials.

Cytotoxicity properties are based on the CD_{50}, as the cell viability was below 50%, the material is toxic [41]. All studied groups showed cell viability higher than 70%, ie., all the synthesized composites are biocompatible and enhance cell proliferation.

In addition, the presence of Ald on HA-Gel-Ald nps showed higher cells viability than those of HA-Gel nps. E. Boanini et al. [56] reported that the Ald-modified groups increases cell viability and improves osteoblast proliferation, cells attachment and spreading [41].

Moreover, HA is the main ingredient of the human bone, could improve the biocompatibility of the nanocomposites. As the concentration of HA decreased, the cells viability increased, which may be attributed to the decrease in Ca^{2+} ions which would inhibit the biocompatibility [45,57].

Conclusion

In conclusion, porous nanocomposites scaffolds, HA-Gel np and HA-Gel-Ald np, were fabricated. These composites have been characterized based on spectral (FTIR, XRD, SEM) and EDX measurements. MTT assay was applied to study the cytotoxicity of the reported nanocomposites. The prepared composites are considered nontoxic and a positive correlation between (HA-Gel np and Ald) content and cell viability was suggested. These biodegradable nanocomposites are expected to be intelligent compounds and the biomimetic composite scaffold of HA-Gel-Ald np could be suggested as a promising material to promote osteoblast cell growth in bone tissue engineering.

Declarations

Funding

This research is funded by the High Ministry of Education, Post 2014 and BRIDGES-Development-3 Project, Scientific Research Academy, Ministry of Research, Egypt.

Acknowledgments

The authors are thankful to the Egyptian High Ministry of Education.

Conflicts of Interest

The authors declare no conflict of interest. This work is original research that has not been published previously and not under consideration for publication elsewhere. All the authors listed have approved the manuscript that is enclosed. All figures in this manuscript are non-published and original. There are no personal circumstances or interest that may be perceived as inappropriately influencing the representation or interpretation of reported research results. The funders had no role in the design of the study; in the collection, analyses, or interpretation of data; in the writing of the manuscript, or in the decision to publish the results.

References

1. Delmas PD (2005) The treatment of postmenopausal osteoporosis. Prevention and Treatment of Osteoporosis in the High-Risk Patient. CRC Press, pp 58–82
2. Datta N, Pham QP, Sharma U, Sikavitsas VI, Jansen JA, Mikos AG (2006) In vitro generated extracellular matrix and fluid shear stress synergistically enhance 3D osteoblastic differentiation. Proc Natl Acad Sci USA 103(8):2488–2493
3. Mao J, Giannobile W, Helms J, Hollister S, Krebsbach P, Longaker M et al (2006) Craniofacial tissue engineering by stem cells. J Dent Res 85(11):966–979
4. Lanza R, Langer R, Vacanti JP (2011) Principles of tissue engineering. Academic press
5. Mao J, Vunjak-Novakovic G, Mikos A, Atala A (2007) : 1–3
6. Murugan R, Ramakrishna S (2004) Bioresorbable composite bone paste using polysaccharide based nano hydroxyapatite. Biomaterials 25(17):3829–3835
7. Putra AP, Hikmawati D, Budiatin AS (2019) Injectable Bone Substitute of Hydroxyapatite-Gelatin Composite with Alendronate for Bone Defect Due to Osteoporosis. J Int Dent Med Res 12(2):813–818
8. Azami M, Rabiee M, Moztarzadeh F (2010) Glutaraldehyde crosslinked gelatin/hydroxyapatite nanocomposite scaffold, engineered via compound techniques. Polym Compos 31(12):2112–2120

9. Gueldner SH, Grabo TN, Newman ED, Cooper DR (2007) Osteoporosis: clinical guidelines for prevention, diagnosis, and management. Springer Publishing Company, pp 9–18
10. Wahl D, Czernuszka J (2006) Collagen-hydroxyapatite composites for hard tissue repair. Eur Cell Mater 11(1):43–56
11. Chang MC, Ko C-C, Douglas WH (2003) Preparation of hydroxyapatite-gelatin nanocomposite. Biomaterials 24(17):2853–2862
12. Rusu VM, Ng C-H, Wilke M, Tiersch B, Fratzl P, Peter MG (2005) Size-controlled hydroxyapatite nanoparticles as self-organized organic–inorganic composite materials. Biomaterials 26(26):5414–5426
13. Zarif M-E (2018) A review of chitosan-, alginate-, and gelatin-based biocomposites for bone tissue engineering. Biomater Tissue Eng Bull 5:97–109
14. Jalise SZ, Baheiraei N, Bagheri F (2018) The effects of strontium incorporation on a novel gelatin/bioactive glass bone graft: In vitro and in vivo characterization. Ceram Int 44(12):14217–14227
15. Mao D, Li Q, Li D, Tan Y, Che Q, Zarif M (2018) A review of chitosan-, alginate-, and gelatin-based biocomposites for bone tissue engineering, Biomaterials and Tissue Engineering Bulletin, 2018, 5 (3–4): 97–109
16. ASKAR ZK, Ourang F, Moztarzadeh F (2005) Fabrication and characterization of a porous composite scaffold based on gelatin and hydroxyapatite for bone tissue engineering.
17. Zhang J, Liu G, Wu Q, Zuo J, Qin Y, Wang J (2012) Novel mesoporous hydroxyapatite/chitosan composite for bone repair. J Bionic Eng 9(2):243–251
18. Zima A (2018) Hydroxyapatite-chitosan based bioactive hybrid biomaterials with improved mechanical strength. Spectrochim Acta Part A Mol Biomol Spectrosc 193:175–184
19. Echave M, Sánchez P, Pedraz J, Orive G (2017) Progress of gelatin-based 3D approaches for bone regeneration. J Drug Deliv Sci Technol 42:63–74
20. Farokhi M, Mottaghitalab F, Samani S, Shokrgozar MA, Kundu SC, Reis RL et al (2018) Silk fibroin/hydroxyapatite composites for bone tissue engineering. Biotechnol Adv 36(1):68–91
21. Gašparič P, Kurečič M, Kargl R, Maver U, Gradišnik L, Hribernik S et al (2017) Nanofibrous polysaccharide hydroxyapatite composites with biocompatibility against human osteoblasts. Carbohydr Polym 177:388–396
22. Kutikov AB, Song J (2013) An amphiphilic degradable polymer/hydroxyapatite composite with enhanced handling characteristics promotes osteogenic gene expression in bone marrow stromal cells. Acta Biomater 9(9):8354–8364
23. Kim H, Che L, Ha Y, Ryu W (2014) Mechanically-reinforced electrospun composite silk fibroin nanofibers containing hydroxyapatite nanoparticles. Mater Sci Engineering: C 40:324–335
24. Lian H, Zhang L, Meng Z (2018) Biomimetic hydroxyapatite/gelatin composites for bone tissue regeneration: Fabrication, characterization, and osteogenic differentiation in vitro. Mater Design

156:381–388
25. Langston AL, Ralston S (2004) Management of Paget's disease of bone. Rheumatology 43(8):955–959
26. Abdou WM, Shaddy AA, Li W, Zhou J, Xu Y (2009) Study of the in vitro cytotoxicity testing of medical devices. Biomedical reports. 2015;3(5):617 – 20
27. Fleisch HA (1997) Bisphosphonates: preclinical aspects and use in osteoporosis. Ann Med 29(1):55–62
28. Body J-J, Bartl R, Burckhardt P, Delmas P, Diel I, Fleisch H et al (1998) Current use of bisphosphonates in oncology. International Bone and Cancer Study Group. J Clin Oncol 16(12):3890–3899
29. Duque G, Rivas D (2007) Alendronate has an anabolic effect on bone through the differentiation of mesenchymal stem cells. J Bone Miner Res 22(10):1603–1611
30. Giger EV, Castagner B, Leroux J-C (2013) Biomedical applications of bisphosphonates. J Controlled Release 167(2):175–188
31. Shi X, Wang Y, Ren L, Gong Y, Wang D-A (2009) Enhancing alendronate release from a novel PLGA/hydroxyapatite microspheric system for bone repairing applications. Pharm Res 26(2):422–430
32. Bauer L, Antunović M, Rogina A, Ivanković M, Ivanković H (2021) Bone-mimetic porous hydroxyapatite/whitlockite scaffolds: preparation, characterization and interactions with human mesenchymal stem cells. J Mater Sci 56(5):3947–3969
33. Sabry AaA, Salih NA (2020) Synthetic Properties of Hydroxyapatite Powder Prepared from Natural Eggs shell. J Gr Eng 10(7):3498–3507
34. Jakab M, Enisz-Bódogh M, Makó É, Kovács K, Orbán S, Horváth B (2020) Influence of wet chemical processing conditions on structure and properties of magnetic hydroxyapatite nanocomposites. Process Application Ceram 14(4):321–328
35. Sinha A, Nayar S, Agrawal A, Bhattacharyya D, Ramachandrarao P (2003) Synthesis of nanosized and microporous precipitated hydroxyapatite in synthetic polymers and biopolymers. J Am Ceram Soc 86(2):357–359
36. Kailasanathan C, Selvakumar N (2012) Comparative study of hydroxyapatite/gelatin composites reinforced with bio-inert ceramic particles. Ceram Int 38(5):3569–3582
37. Rapacz-Kmita A, Paluszkiewicz C, Ślósarczyk A, Paszkiewicz Z (2005) FTIR and XRD investigations on the thermal stability of hydroxyapatite during hot pressing and pressureless sintering processes. J Mol Struct 744:653–656
38. Reyes-Gasga J, Martínez-Piñeiro EL, Rodríguez-Álvarez G, Tiznado-Orozco GE, García-García R, Brès EF (2013) XRD and FTIR crystallinity indices in sound human tooth enamel and synthetic hydroxyapatite. Mater Sci Engineering: C 33(8):4568–4574

39. Li B, Nasiri-Tabrizi B, Baradaran S, Yeong CH, Basirun WJ (2021) Ultrasonic-assisted preparation of reduced graphene oxide-hydroxyapatite nanocomposite for bone remodeling. Mater Lett 284:128990
40. Ferraris S, Yamaguchi S, Barbani N, Cazzola M, Cristallini C, Miola M et al (2020) Bioactive materials: In vitro investigation of different mechanisms of hydroxyapatite precipitation. Acta Biomater 102:468–480
41. Putra AP, Rahmah AA, Fitriana N, Rohim SA, Jannah M, Hikmawati D (eds) (2018) The effect of glutaraldehyde on hydroxyapatite-gelatin composite with addition of alendronate for bone filler application. Journal of Biomimetics, Biomaterials and Biomedical Engineering; : Trans Tech Publ
42. Zare Jalise S, Baheiraei N, Bagheri F (2018) The effects of strontium incorporation on a novel gelatin/bioactive glass bone graft: In vitro and in vivo characterization. Ceram Int 44:14217–14227
43. Sobhi BM, Ismael EY, Mansour AS, Elsabagh M, Fahmy KN (2020) Effect of Nano-hydroxyapatite as an Alternative to Inorganic Dicalcium Phosphate on Growth Performance, Carcass Traits, and Calcium and Phosphorus Metabolism of Broiler Chickens. J Adv Veterinary Res 10(4):250–256
44. Chen P, Liu L, Pan J, Mei J, Li C, Zheng Y (2019) Biomimetic composite scaffold of hydroxyapatite/gelatin-chitosan core-shell nanofibers for bone tissue engineering. Mater Sci Engineering: C 97:325–335
45. Chen X, Wu D, Xu J, Yan T, Chen Q (2021) Gelatin/Gelatin-modified nano hydroxyapatite composite scaffolds with hollow channel arrays prepared by extrusion molding for bone tissue engineering. Mater Res Express 8(1):015027
46. Hossan MJ, Gafur MA, Kadir MR, Karima MM (2014) Preparation and Characterization of GelatinHydroxyapatite Composite for Bone Tissue Engineering. Int J Eng Technol 14(1):24–32
47. Fathy AA, Butler IS, Abd Elrahman M, Jean-Claude BJ, Mostafa SI (2018) Anticancer evaluation and drug delivery of new palladium (II) complexes based on the chelate of alendronate onto hydroxyapatite nanoparticles. Inorg Chim Acta 473:44–50
48. Fathy A, Butler I, Elrahman M (2017) New Active Bisphosphonate (Etidronate) Complexes as Anticancer Agents. Inorg Chem Ind J 12(2):119
49. Putra AP, Faradisa I, Hikmawati D (eds) (2019) The Effect of Hydroxyapatite-Gelatin Composite with Alendronate as Injectable Bone Substitute on Various Hydroxyapatite-Based Substrate. 2019 International Biomedical Instrumentation and Technology Conference (IBITeC); : IEEE
50. Arunseshan C, Suresh S, Arivuoli D (2013) Synthesis and characterization of nano-hydroxyapatite (n-HAP) using the wet chemical technique. Int J Phys Sci 8(32):1639–1645
51. Tomšová K, Ďurovič M, Drábková K (2016) The effect of disinfection methods on the stability of photographic gelatin. Polym Degrad Stab 129:1–6
52. Neamtu J, Bubulica MV, Rotaru A, Ducu C, Balosache OE, Manda VC et al (2017) Hydroxyapatite–alendronate composite systems for biocompatible materials. J Therm Anal Calorim 127(2):1567–1582
53. Monshi A, Foroughi MR, Monshi MR (2012) Modified Scherrer Equation to Estimate More Accurately Nano-Crystallite Size Using XRD. World J Nano Sci Eng 2(3):154–160. DOI:

10.4236/wjnse.2012.23020

54. Boanini E, Gazzano M, Rubini K, Bigi A (2007) Composite nanocrystals provide new insight on alendronate interaction with hydroxyapatite structure. Adv Mater 19(18):2499–2502
55. Boanini E, Torricelli P, Gazzano M, Fini M, Bigi A (2012) The effect of zoledronate-hydroxyapatite nanocomposites on osteoclasts and osteoblast-like cells in vitro. Biomaterials 33(2):722–730
56. Boanini E, Torricelli P, Gazzano M, Giardino R, Bigi A (2008) Alendronate–hydroxyapatite nanocomposites and their interaction with osteoclasts and osteoblast-like cells. Biomaterials 29(7):790–796
57. Shalumon K, Lai G-J, Chen C-H, Chen J-P (2015) Modulation of bone-specific tissue regeneration by incorporating bone morphogenetic protein and controlling the shell thickness of silk fibroin/chitosan/nanohydroxyapatite core–shell nanofibrous membranes. ACS Appl Mater Interfaces 7(38):21170–21181

Tables

Table 1: Crystal size (nm) of the prepared nanocomposite

Groups	Crystal size (nm)	Groups	Crystal size (nm)
G1	51.2	G4	27.2
G2	67.75	G5	36.8
G3	74	G6	46.7

Table 2: Descriptive statistics and comparison of cell proliferation between groups (ANOVA test)

Cell proliferation	Mean	SD	F	P
G1	73.37[d]	0.52		
G2	75.17[d]	0.38	258.3	.000*
G3	74.27[d]	1.07		
G4	93.68[a]	0.52		
G5	95.50[a]	0.82		
G6	93.14[a,b]	1.10		

*Significance level p≤0.05, *significant*

Tukey's post hoc test: means sharing the same superscript letter are not significantly different

Table 3: Results of two ways ANOVA test for interaction of composition and concentration variables regarding cytotoxicity

Source	Type III Sum of Squares	df	Mean Square	F	P value
Composition	1917.900	2	958.950	1020.763	.000*
Concentration	20.826	2	10.413	11.084	.001*
Composition * Concentration	2.502	4	.626	.666	.624ns
Error	16.910	18	.939		
Total	200899.206	27			
Corrected Total	1958.139	26			

*Significance level p≤0.05, *significant, ns= non-significant*

Figures

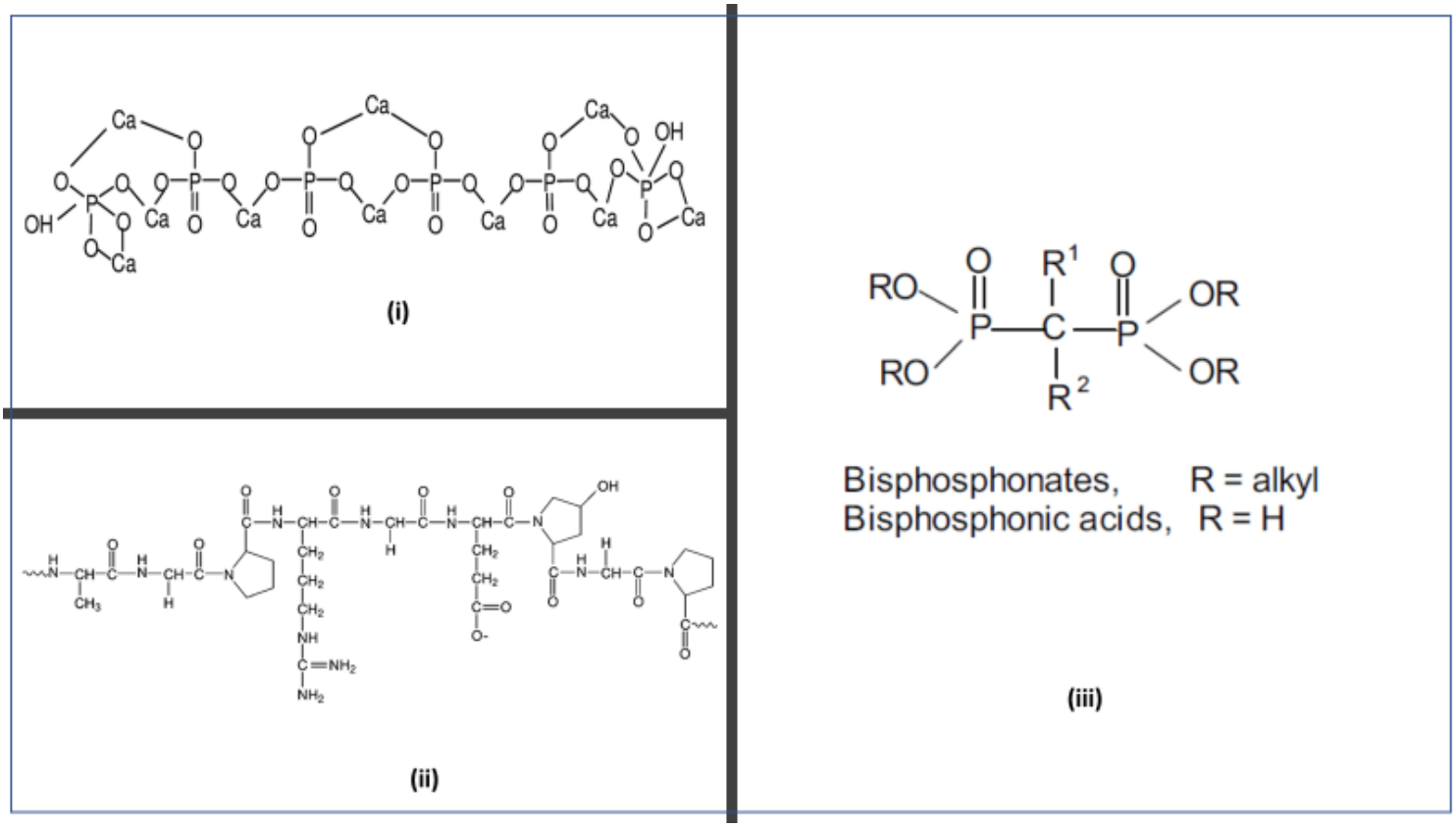

Figure 1

Structure of HA (i), Gel (ii) and Bps (iii)

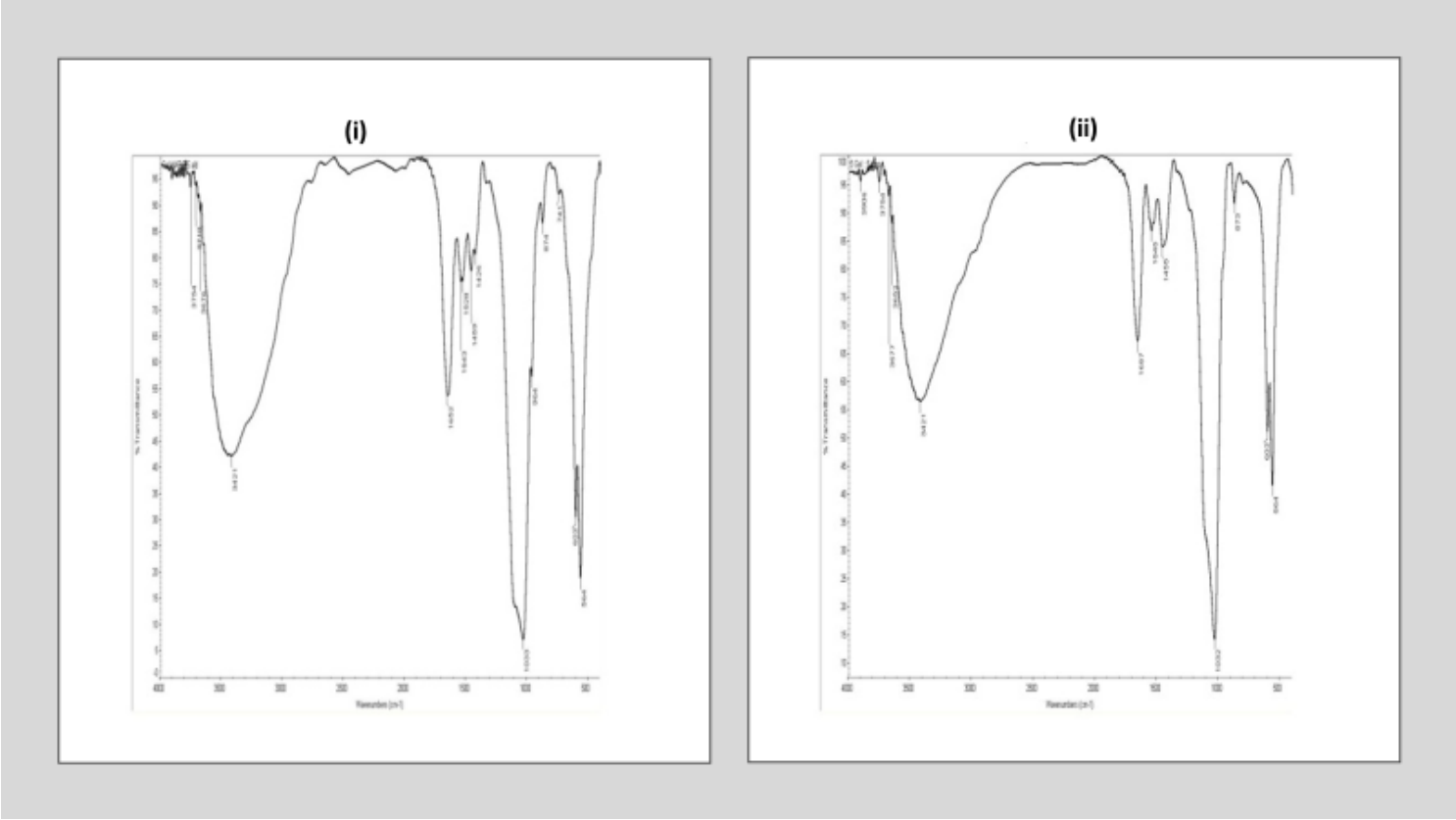

Figure 2

IR spectra of HA-Gel np (1:1; i) and HA-Gel-Ald np (1: 1; ii)

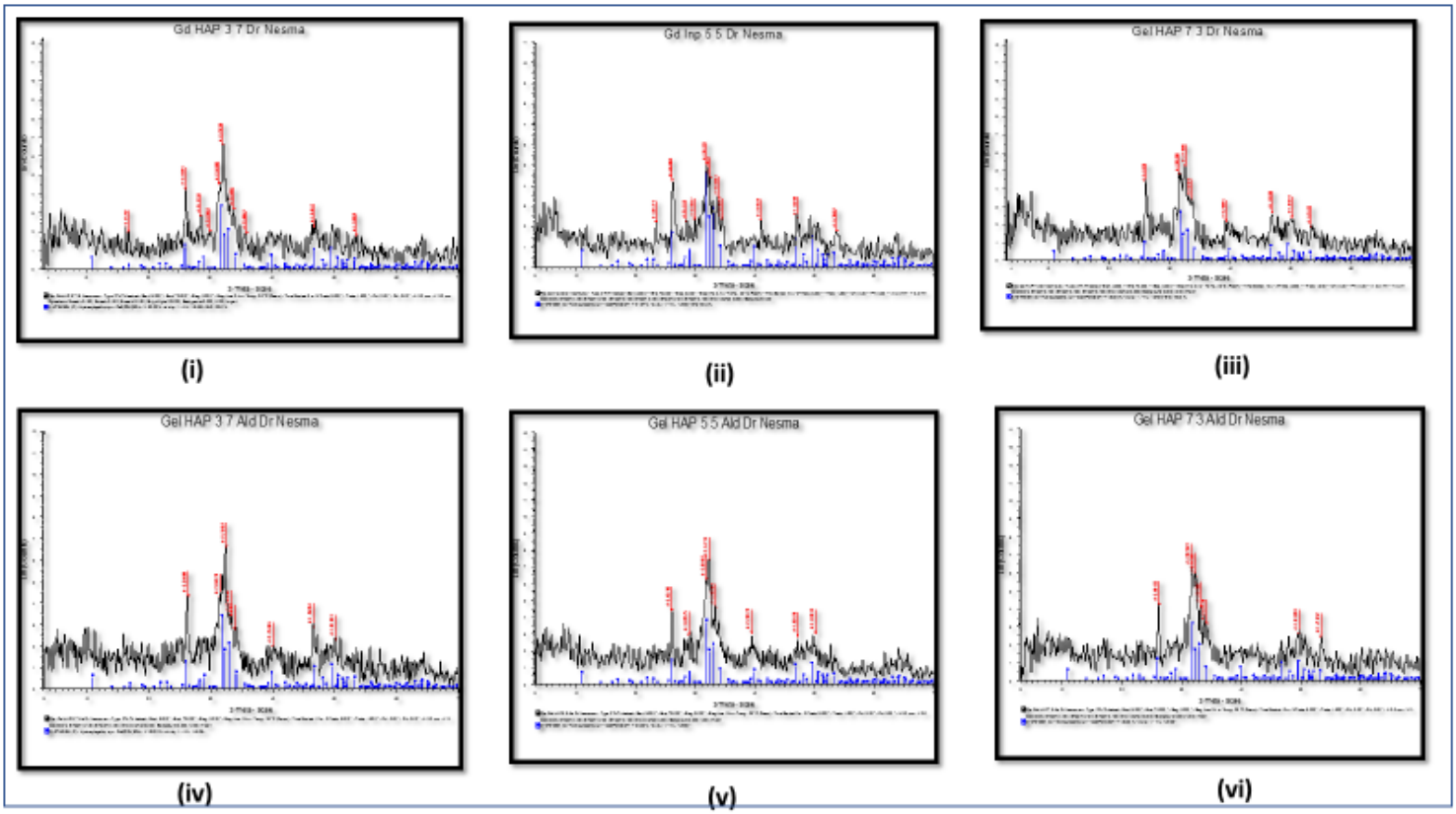

Figure 3

XRD patterns of HA-Gel np (7:3; i), HA-Gel np (1:1; ii), HA-Gel np (3:7; iii), HA-Gel-Ald np (7:3; iv), HA-Gel-Ald np (1: 1; v) and HA-Gel-Ald np (3:7; vi).

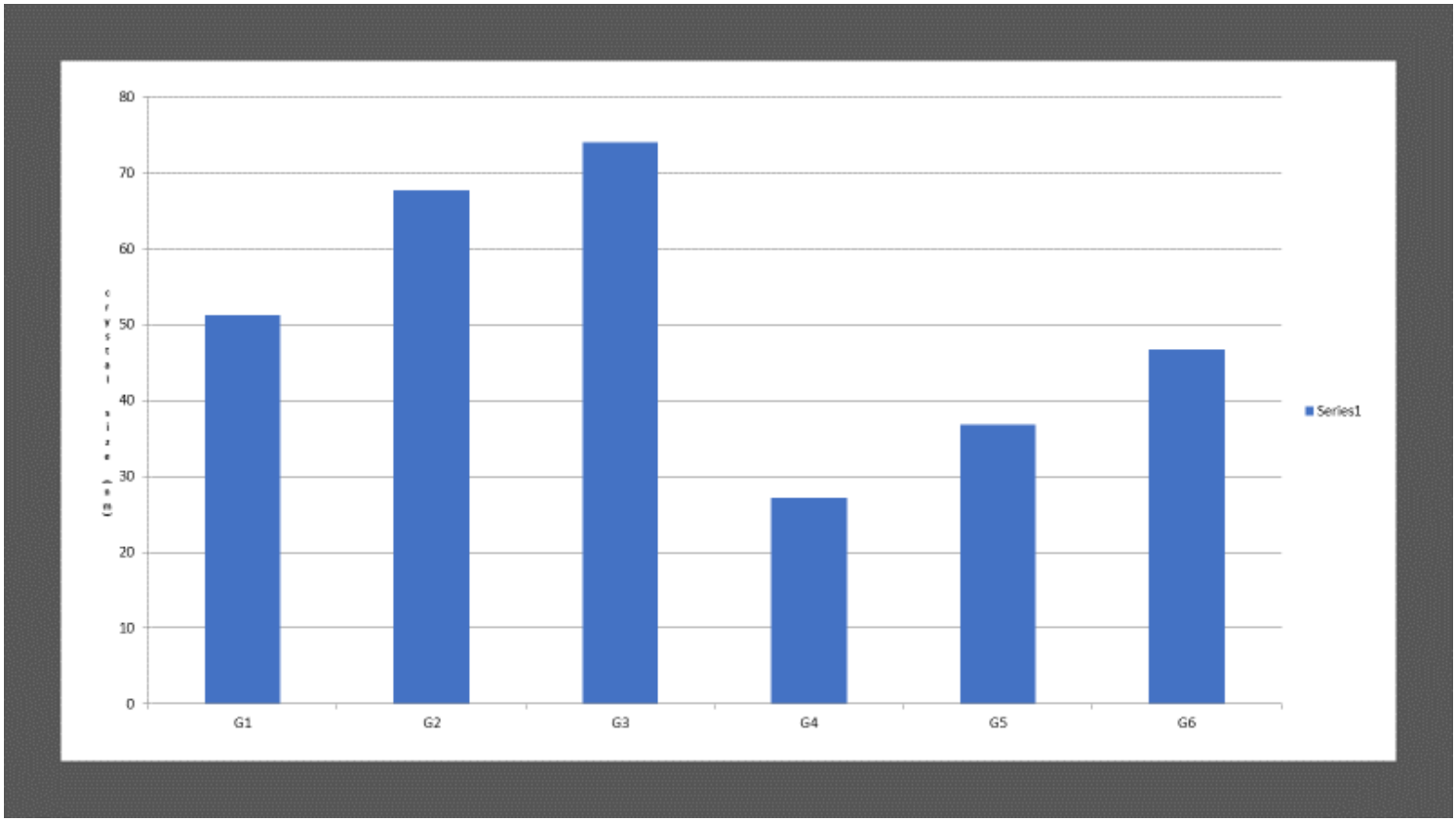

Figure 4

Crystal sizes (nm) of HA-Gel np (7:3; i), HA-Gel np (1:1; ii), HA-Gel np (3:7; iii), HA-Gel-Ald np (7:3; iv), HA-Gel-Ald np (1: 1; v) and HA-Gel-Ald np (3:7; vi).

nanocomposites

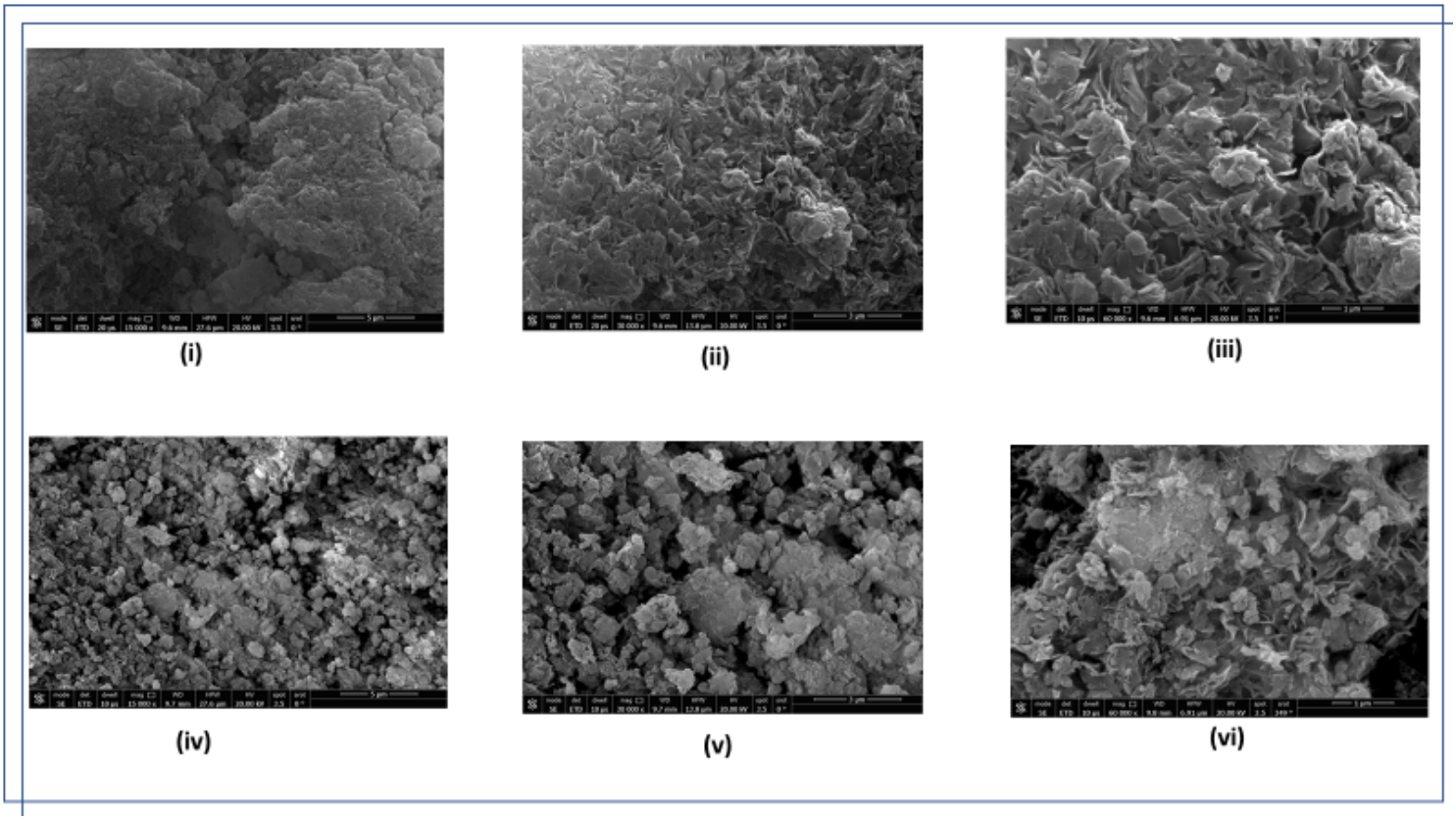

Figure 5

SEM images of HA-Gel np (7:3; i), HA-Gel np (1:1; ii), HA-Gel np (3:7; iii), HA-Gel-Ald np (7:3; iv), HA-Gel-Ald np (1: 1; v) and HA-Gel-Ald np (3:7; vi).

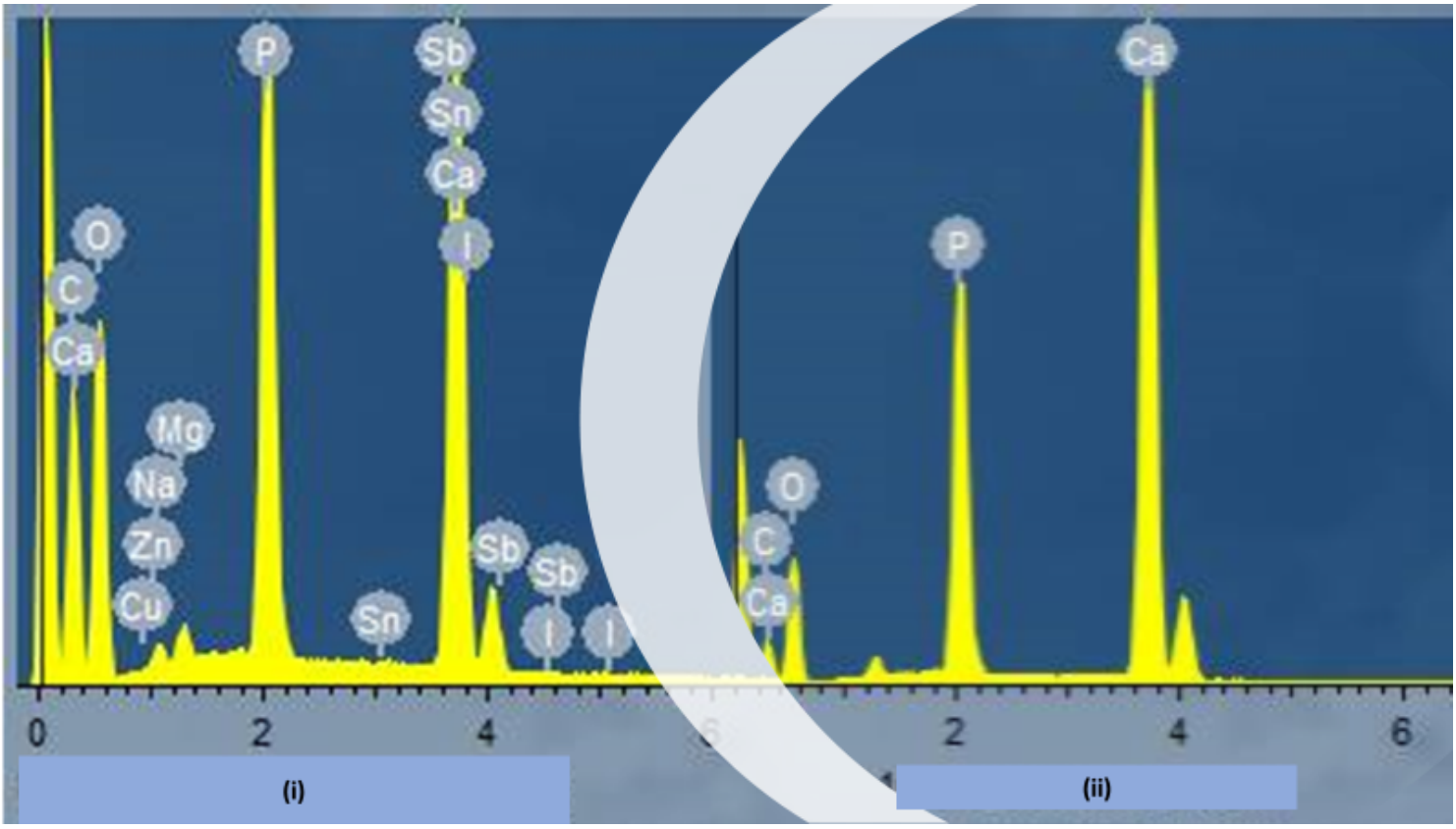

Figure 6

EDX of HA-Gel np (1:1; i) and HA-Gel-Ald np (1:1; ii).

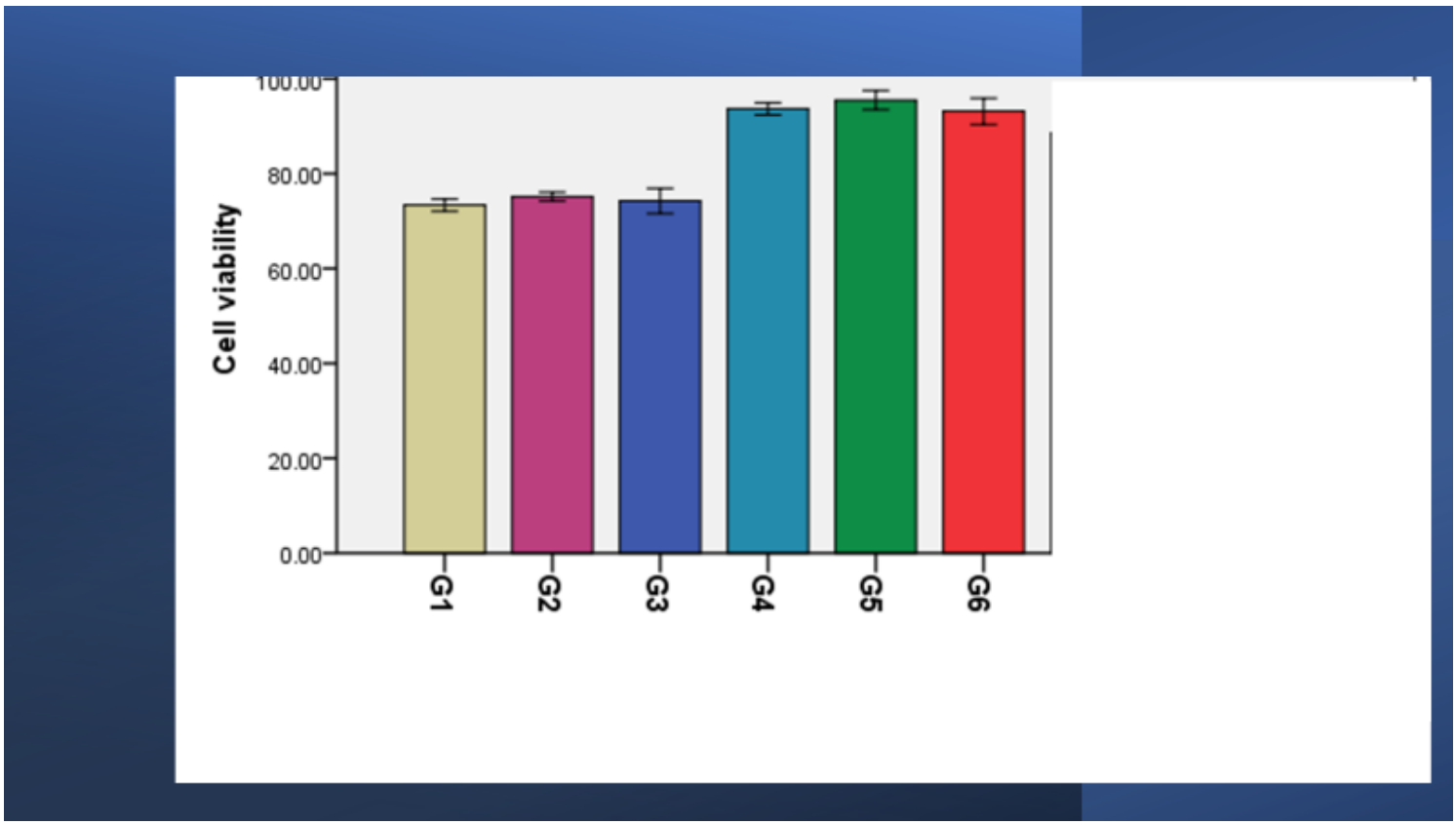

Figure 7

Cell viability (%) (using MTT assay) for the nanocomposites, HA-Gel np (7:3; G1), HA-Gel np (1:1; G2), HA-Gel np (3:7; G3), HA-Gel-Ald np (7:3; G4), HA-Gel-Ald np (1: 1; G5) and HA-Gel-Ald np (3:7; G6).

Supplementary Files

This is a list of supplementary files associated with this preprint. Click to download.

- GraphicalAbstract.docx